

GALAXY CLUSTERS AT HIGH REDSHIFT AND EVOLUTION OF BRIGHTEST CLUSTER GALAXIES

Z. L. WEN, J. L. HAN

National Astronomical Observatories, Chinese Academy of Sciences, 20A Datun Road, Chaoyang District, Beijing 100012, China; zhonglue@nao.cas.cn.

Received 2011 January 2; accepted 2011 April 7; published 2011 May 25 on ApJ 734, 68.

ABSTRACT

Identification of high redshift clusters is important for studies of cosmology and cluster evolution. Using photometric redshifts of galaxies, we identify 631 clusters from the Canada-France-Hawaii Telescope (CFHT) Wide field, 202 clusters from the CHFT Deep field, 187 clusters from the Cosmic Evolution Survey (COSMOS) and 737 clusters from the Spitzer Wide-area InfraRed Extragalactic survey (SWIRE) field. The redshifts of these clusters are in the range of $0.1 \lesssim z \lesssim 1.6$. Merging these cluster samples gives 1644 clusters in the four survey fields, of which 1088 are newly identified and more than half are from the large SWIRE field. Among 228 clusters of $z \geq 1$, 191 clusters are newly identified, and most of them from the SWIRE field. With this large sample of high redshift clusters, we study the color evolution of the brightest cluster galaxies (BCGs). The colors $r' - z'$ and $r^+ - m_{3.6\mu m}$ of the BCGs are consistent with a stellar population synthesis model in which the BCGs are formed at redshift $z_f \geq 2$ and evolved passively. The colors $g' - z'$ and $B - m_{3.6\mu m}$ of the BCGs at redshifts $z > 0.8$ are systematically bluer than the passive evolution model for galaxy formed at $z_f \sim 2$, indicating star formation in high redshift BCGs.

Subject headings: galaxies: clusters: general — galaxies: elliptical and lenticular, cD — galaxies: evolution

1. INTRODUCTION

Galaxy clusters are important objects to study the large scale structure (Bahcall 1988; Postman et al. 1992) and constraint the cosmological parameters, e.g., Ω_m , the mass density parameter of the universe, and σ_8 , the amplitude of mass fluctuations at a scale of $8 h^{-1}$ Mpc (Bahcall et al. 1997; Reiprich & Böhringer 2002; Wen et al. 2010). Clusters are also important laboratories to investigate the properties of dark matter, hot gas, galaxies and active galactic nucleus in dense environment (e.g., Castillo-Morales & Schindler 2003; Dressler 1980; Croft et al. 2007). However, most of these investigations are based on clusters in the local universe.

High redshift clusters can provide information on cosmological structure in the vast universe and the evolution of cluster properties with cosmic time. It has been shown that cluster galaxies at high redshift have more star formation than those at low redshift (Butcher & Oemler 1978, 1984). The evolution of cluster mass functions gives constraints on not only the cosmological parameters but also dark energy equation of state parameter ω_0 (e.g., Vikhlinin et al. 2009). The abundance of (even a few) high redshift massive clusters constrains the non-Gaussianity of primordial perturbation (Matarrese et al. 2000; Hoyle et al. 2010). High redshift clusters are needed to study the formation and evolution of brightest cluster galaxies (Miley et al. 2006; Whiley et al. 2008; Stott et al. 2008).

1.1. Previous detection of high redshift clusters

Tens of thousands of galaxy clusters have been identified from various surveys in the last decades (e.g., Abell et al. 1989; Wen et al. 2009; Hao et al. 2010). They mostly have redshifts $z < 0.5$. High redshift clusters were recently identified from multi-color optical or infrared deep surveys. Only a few hundreds of clusters have redshifts $z > 1$ (e.g., Gladders & Yee 2005; Goto et al. 2008).

Using cluster red sequence method, Gladders & Yee (2005) detected 429 candidate clusters or groups with redshifts of $0.2 < z < 1.4$ from the Red-Sequence Cluster Survey (RCS), of which 67 have $0.9 < z < 1.4$. Using the Cut and En-

hance method, Goto et al. (2008) identified 16 cluster candidates at redshifts $0.9 < z < 1.7$ from the AKARI deep survey. Eisenhardt et al. (2008) used a wavelet algorithm based on photometric redshift to the Spitzer Infrared Array Camera (IRAC) Shallow Survey and NAO Deep Wide-Field Survey data and identified 335 cluster and group candidates, of which 106 have redshifts $z \geq 1$.

Olsen et al. (2007) applied a matched-filter cluster detection algorithm to the Canada-France-Hawaii Telescope Legacy Survey (CFHTLS). They identified 162 cluster candidates over an area of 3.112 deg^2 , of which 29 have redshifts $z \geq 1$. Grove et al. (2009) found 114 cluster candidates by using a matched filter detection method to the CFHTLS r' band data of the Deep fields, and 247 cluster candidates from the z' band data. Merging the samples in both bands gives 233 clusters, of which 93 have redshifts $z \geq 1$. Thanjavur et al. (2009) found 5804 cluster candidates from the CFHT Wide field of 161 deg^2 using the red sequence method, of which 13 have redshifts $z \geq 1$. By mapping density of galaxy distribution in photometric redshift space, Adami et al. (2010) detected 1200 candidate clusters with masses greater than $1.0 \times 10^{13} M_\odot$ from the CFHTLS Deep and Wide fields, of which 302 have redshifts $z \geq 1$. Milkeraitis et al. (2010) applied a 3-dimensional matched-filter cluster detection algorithm to the CFHTLS data and identified 673 cluster candidates in the redshift range of $0.2 \leq z \leq 1.0$.

Knobel et al. (2009) used the friends-of-friends and Voronoi tessellation methods and identified 102 groups of $z \leq 1$ with more than five member galaxies from $\sim 10,000$ redshifts from the Cosmic Evolution Survey (COSMOS) field. van Breukelen et al. (2006) identified 13 clusters in the redshift range of $0.61 \leq z \leq 1.39$ from the UKIRT Infrared Deep Sky Survey (UKIDSS) Early Data Release. Zatloukal et al. (2007) identified 12 cluster candidates in the redshift range of $1.23 \leq z \leq 1.55$ from the Heidelberg InfraRed/Optical Cluster Survey (HIROCS) survey in the COSMOS field. Chiaberge et al. (2010) found three candidate clusters of galaxies at redshifts most likely between 1.7 and 2.0 in the COSMOS field. Wang et al. (2010) used the friend-

of-friend method to the Great Observatories Origins Deep Survey (GOODS) data and identified 206 group at redshift between 0.4 and 1.0. From the first 36 XMM-Newton pointings on the COSMOS field, Finoguenov et al. (2007) identified 72 clusters, of which 8 have redshifts $z \geq 1$. From the XMM-LSS survey, Pierre et al. (2007) identified 73 clusters. From the Subaru-XMM Deep Field, Finoguenov et al. (2010) identified 57 cluster candidates, of which 13 have redshifts $z \geq 1$.

Besides the sample finding, some authors have spectroscopically found or confirmed individual high redshift clusters. Kurk et al. (2009) confirmed a galaxy cluster of $z = 1.6$ from the Galaxy Mass Assembly ultra-deep Spectroscopic Survey (GMASS). Gilbank et al. (2008) confirmed a compact supercluster structure comprising three clusters at $z = 0.9$. Papovich et al. (2010) discovered a galaxy cluster at $z = 1.62$ from the Spitzer Wide-Area Infrared Extragalactic survey (SWIRE) XMM-LSS field. Andreon et al. (2008) confirmed a cluster at $z = 1.016$ using a modified red sequence method, follow up spectroscopy and X-ray imaging. From the Spitzer/IRAC Shallow Survey of the Bootes field, Stanford et al. (2005) confirmed a galaxy cluster at $z = 1.41$. From the Spitzer Adaptation of the Red-sequence Cluster Survey (SpARCS), Muzzin et al. (2009), Wilson et al. (2009) and Demarco et al. (2010) confirmed two clusters at $z \sim 1.2$, one cluster at $z = 1.34$ and three cluster at $z = 0.87, 1.16, 1.21$, respectively. Using a 3-dimensional technique, Castellano et al. (2007) detected a forming galaxy cluster at redshift 1.6 in the GOODS field. A few high redshift massive clusters were found by X-ray observations and Sunyaev-Zeldovich (SZ) effect. From the XMM-Newton observations, a massive X-ray cluster at $z = 1.39$ was discovered by Mullis et al. (2005) and a massive X-ray cluster at $z = 1.45$ by Stanford et al. (2006), and a cluster at $z = 1.22$ was identified by Bremer et al. (2006) and a cluster at $z = 0.95$ by Fassbender et al. (2008). Using the SZ effect, Brodwin et al. (2010) found a massive cluster at $z = 1.07$ from the South Pole Telescope (SPT) data.

1.2. Evolution of brightest cluster galaxies

The brightest cluster galaxy (BCG) is an elliptical galaxy located at the potential center of a galaxy cluster. BCGs are the most luminous galaxies in the universe and *in general* have no prominent ongoing star formation. They are red in the rest-frame color. Their surface brightness profiles are different from those of ordinary elliptical galaxies (non-BCGs), and they do not follow the basic scaling relations of normal ellipticals (e.g., Lauer et al. 2007; Liu et al. 2008). Because of the dominant role inside clusters and their unusual properties, the formation and evolution of BCGs are very intriguing.

The properties and evolution of BCGs were studied using identified high redshift clusters. Bernardi (2009) noticed that BCGs at lower redshift have larger sizes and smaller velocity dispersions, indicating that early-type BCGs grow from many dry minor mergers (Miley et al. 2006) rather than a few major mergers (Rines et al. 2007). By comparing the structural parameters of BCGs of nearby clusters ($0.04 < z < 0.07$) and those at intermediate redshift ($0.3 < z < 0.6$), Ascaso et al. (2011) confirmed the size decrease of BCGs with redshift. The properties of BCGs are related to the host clusters. More luminous, larger and more centrally located BCGs are located in more massive and rich galaxy clusters.

On the K -band Hubble diagram, BCGs do not exhibit any luminosity evolution with redshift (Collins & Mann 1998; Aragon-Salamanca et al. 1998; Whiley et al. 2008) and sig-

nificant change in the stellar mass (Whiley et al. 2008). The colors of BCGs are in good agreement with the evolved old stellar population formed at $z > 2$. This means that the stellar population in BCGs has been in place since at least $z = 2$ (Stott et al. 2008) and the average stellar mass of BCGs remains constant since $z \sim 1.5$. Stott et al. (2010) therefore concluded that dry merger seems to have little effect on evolutions of BCG stellar mass over the last 9 – 10 Gyr.

However, Liu et al. (2009) found that dry merger plays an important role in the stellar mass assembly of BCGs. De Lucia & Blaizot (2007) concluded from hierarchical simulations that the half mass of a typical BCG is assembled by dry mergers after $z \sim 0.5$. The stellar populations of BCGs are formed very early, 50% at redshift $z \sim 5$ and 80% at $z \sim 3$.

Observationally, a very small number of BCGs, e.g., those in Abell 1835, Zw3146 and MACS J0913.7+4056, exceptionally show the features of star formation (McNamara et al. 2006; Egami et al. 2006; Bildfell et al. 2008; O’Dea et al. 2008; Donahue et al. 2010; Hicks et al. 2010) or post-starburst features (Liu et al. 2011). The star formation is the dominant power for the infrared and $H\alpha$ emission detected from BCGs (O’Dea et al. 2008).

As shown above, many controversies exist on the formation of BCGs and the role of dry merger (Liu et al. 2009; Stott et al. 2010). It is not clear when the BCGs are formed, what process dominates the evolution of BCGs. Finding more high redshift clusters and their BCGs is crucial to study these questions.

In this paper, we identify high redshift clusters from the CFHT Wide field, the CHFT Deep field, the COSMOS field and the Spitzer SWIRE field. In Section 2, we first apply our cluster detection algorithm to the photometric redshift data of the four fields, and identify high-redshift clusters. We then discuss the false detection rate, the accuracy of determined cluster redshift, cluster richness and X-ray luminosity of some clusters. The color evolution of BCGs is studied in Section 3. Conclusions of this paper are presented in Section 4.

Throughout this paper, we assume a Λ CDM cosmology by taking $H_0 = 100 h \text{ km s}^{-1} \text{ Mpc}^{-1}$, with $h = 0.72$, $\Omega_m = 0.3$ and $\Omega_\Lambda = 0.7$.

2. HIGH REDSHIFT CLUSTERS DETECTED FROM DEEP FIELDS

To identify high redshift clusters, one has to discriminate the cluster member galaxies from field galaxies in deep fields. Note that the projection effect is very serious in photometric data. The “color cut” (Goto et al. 2008) or “red sequence” (Gladders & Yee 2005) methods have been previously used for de-projection. Galaxy clusters can be detected in a certain redshift range when proper filters covering the 4000Å break feature are used for photometry. When the break feature shifts out from the chosen filters, photometric data of other bands must be used for color cuts. Cluster richness determined by different color cuts may not match well (e.g. Hao et al. 2010). The enhanced star formation in galaxies of high redshift clusters (i.e. the Butcher-Oemler effect) also makes the cluster detection more difficult by the color cuts.

The photometric redshifts of galaxies (photo- z) are determined by comparison of the multi-band photometric data with the spectral energy distribution of galaxies including the 4000Å break feature (e.g. Csabai et al. 2003). The photometric redshifts have successfully been used for the de-projection (e.g., Eisenhardt et al. 2008; Wen et al. 2009; Milkeraitis et al. 2010; Adami et al. 2010; Gillis & Hudson

TABLE 1
DETAILS OF THE FOUR DEEP SURVEYS USED FOR IDENTIFICATION OF CLUSTERS.

name	field (deg ²)	mag. limit	No. of bands	$\sigma_{\Delta z}/(1+z)$	photo- z ref.	M_{lim} this paper	No. of clusters	No. of new clusters	No. of high- z clusters	No. of high- z new clusters
CFHT Wide	35.0	$i' < 22.5$	5	0.038	1	$M_{i'} \leq -21.5$	631	285	24	19
CFHT Deep	3.2	$i' < 24$	5	0.029	1,2	$M_{i'} \leq -21.5$	202	55	53	29
COSMOS	2.0	$i^+ < 25$	30	0.012	3	$M_V \leq -20.5$	187	127	43	38
SWIRE	33.0	$r < 24$	5–12	0.035	4	$M_B \leq -20.5$	737	674	116	106

NOTE. — References for photo- z : (1). Coupon et al. (2009); (2). Ilbert et al. (2006); (3). Ilbert et al. (2009); (4). Rowan-Robinson et al. (2008). Here, high- z means $z \geq 1$.

2011). When photometric redshifts of galaxies are used for identification of clusters, one does not have to consider the color of galaxies and the redshift range. Here, we follow and modify the method described in Wen et al. (2009) to identify high redshift clusters from the CFHT Wide field, the CFHT Deep field, the COSMOS field and the Spitzer SWIRE field.

2.1. Photometric redshift data for deep fields

The photometric redshifts of galaxies have been estimated for many multi-color deep surveys, e.g., the GOODS Southern Field (Mobasher et al. 2004), the RCS (Hsieh et al. 2005), the Hubble Ultra Deep Field (Coe et al. 2006), the Spitzer IRAC Shallow Survey (Brodwin et al. 2006), CFHT (Ilbert et al. 2006), SWIRE (Rowan-Robinson et al. 2008), COSMOS (Ilbert et al. 2009), the ESO Distant Cluster Survey field (Pelló et al. 2009), the AKARI survey (Negrello et al. 2009), the Multi-wavelength Survey by Yale-Chile (Cardamone et al. 2010). These surveys provide accurate photometries of 4 to 32 bands from UV to mid-infrared, so that the estimated photometric redshifts have an uncertainty of 0.01 – 0.1. For cluster detection, we restrict the photo- z data with a small uncertainty of $\sigma_{\Delta z} \leq 0.04(1+z)$. In this paper, we work on the deep fields larger than 1 deg². We find that photo- z data for the CFHT Wide field, the CFHT Deep field, the COSMOS field and the Spitzer SWIRE field are available for cluster identification at high redshifts (see details in Table 1).

The CFHT survey is carried out with the 3.6 m Canada-France Hawaii Telescope in the u' , g' , r' , i' and z' bands for three imaging sub-surveys: the CFHT Deep, the CFHT Wide and the CFHT Very Wide. The photo- z data of the Deep and Wide fields have been published and used in previous work (see references in Sect. 1.1). The CFHT Wide survey covers 35 deg² in three deep fields (W1, W3, W4). The CFHT Deep survey covers 3.2 deg² in four deep fields (D1, D2, D3, D4).

The COSMOS is made for a field of 2 deg² by many observations from X-ray to radio (XMM, Galaxy Evolution Explorer, the Hubble Space Telescope, CFHT, United Kindon Infrared Telescope, Subaru, Spitzer and VLA).

The Spitzer SWIRE is to provide photometry (Lonsdale et al. 2003) in the IRAC bands of 3.6 μm , 4.5 μm , 5.8 μm and 8.0 μm , the MIPS bands of 24 μm , 70 μm and 160 μm for six regions: ELAIS-N1, ELAIS-N2, Lockman Hole, XMM, ELAIS-S1 and Chandra Deep Field South (CDFs). The photometries in optical bands u , g , r , i and z (only here is the band, not redshift) are available from the SWIRE photometry programme and from McMahan et al. (2001) and Pierre et al. (2007).

Detailed parameters for the four fields are given in Table 1, including the field size, magnitude limit, number of bands for

photometry, and the accuracy of photo- z .

2.2. Finding high redshift clusters

We identify galaxy clusters using the photo- z data for discrimination of *luminous* member galaxies from the four fields with following steps (Wen et al. 2009):

1. Assuming that each galaxy at a given photometric redshift, z , is the central galaxy of a cluster candidate, we count the number of luminous member galaxies of $M \leq M_{\text{lim}}$, $N(0.5)$, within a radius of 0.5 Mpc and a photo- z gap of $z \pm 1.44 \sigma_{\Delta z}$. See the M_{lim} and $\sigma_{\Delta z}$ values in Table 1. Here, the factor of 1.44 for the photo- z gap is chosen so that more than 85% of member galaxies of a cluster can be included assuming that the uncertainties of photometric redshifts of member galaxies follow a Gaussian distribution. A larger z gap can help to include more member galaxies, but more background galaxies are involved. We set the absolute magnitude limit, not only to make our cluster detection consistent even up to high redshifts, but also to exclude less luminous galaxies as member galaxies which have a larger photo- z uncertainty. The absolute magnitudes of galaxies at the i' -band for the CFHT Wide and the CFHT Deep data, the V -band for the COSMOS data and the B -band for the SWIRE data are provided together with photo- z data of galaxies in their catalogs (Coupon et al. 2009; Ilbert et al. 2009; Rowan-Robinson et al. 2008). The upper limits of absolute magnitude for the four fields are also listed in Table 1. The absolute magnitudes of galaxies are not available for the CFHT Deep field in Ilbert et al. (2006), and we estimate the absolute magnitudes in the i' -band using the K-correction of Fukugita et al. (1995) according to the types of galaxies given by Ilbert et al. (2006).

2. We apply the friend-of-friend algorithm to the luminous galaxies using a linking length of 1 Mpc in the transverse direction and a photo- z gap of $z \pm 3 \sigma_{\Delta z}$. We then find the linked galaxy with the maximum $N(0.5)$ as the temporary center of a cluster candidate. If two or more galaxies show the same maximum number count, the brightest one is taken as the temporary central cluster galaxy. The linking length and photo- z gap are large enough to link all member galaxies in the transverse distance and redshift space. This step can ensure to avoid multiple detection of a cluster.

3. For each galaxy with maximum $N(0.5)$ at z , all galaxies within a radius of 1 Mpc from the temporary central galaxy and the photo- z gap between $z \pm 1.44 \sigma_{\Delta z}$ are assumed to be the member galaxies. The cluster redshift z_p is then defined to be the median value of the photometric redshifts of the recognized “members”. The absolute magnitudes of member galaxies are re-calculated with this cluster redshift.

4. The galaxy overdensity of a cluster, $D = (N(0.5) -$

TABLE 2
CLUSTERS IDENTIFIED FROM THE FOUR DEEP FIELDS.

Name	R.A. _{BCG} (deg)	Decl. _{BCG} (deg)	z_p	$z_{s,BCG}$	mag _{BCG}	D	N_{gal}	R	L_{tot} ($10^{10} L_{\odot}$)	Prev. catalog
(1)	(2)	(3)	(4)	(5)	(6)	(7)	(8)	(9)	(10)	(11)
CFHT-W J021408.5–053410	33.53388	−5.59269	0.4128	−1.0000	18.70	5.77	20	16.00	106.41	1,2
CFHT-W J021527.6–053338	33.86837	−5.55166	0.2848	−1.0000	17.70	9.84	25	23.57	120.67	1,2
CFHT-W J021447.5–053309	33.69700	−5.55293	0.8629	−1.0000	20.83	5.25	25	21.00	186.48	
CFHT-W J021242.9–053219	33.17939	−5.54365	1.1462	−1.0000	22.23	4.55	14	7.43	95.94	
CFHT-D J022435.6–045505	36.13370	−4.91589	0.9846	−1.0000	21.26	4.30	29	19.76	199.19	
CFHT-D J022723.5–045424	36.82425	−4.91559	0.3135	−1.0000	18.95	4.28	16	14.31	73.06	1,2,3
CFHT-D J022624.6–045652	36.59565	−4.95964	0.9416	−1.0000	21.57	5.14	24	19.71	106.97	4
CFHT-D J022425.3–045229	36.09802	−4.87084	0.9458	−1.0000	21.13	4.31	32	21.18	190.84	2,3,5
COSMOS J100313.1+013611	150.81335	1.60198	0.5119	−1.0000	20.25	9.33	15	13.84	49.84	
COSMOS J100117.0+013618	150.34543	1.62183	0.2283	−1.0000	18.74	7.25	13	11.37	33.54	
COSMOS J100112.4+013401	150.28815	1.55581	0.3610	0.3638	19.08	6.47	36	32.15	105.62	6
COSMOS J100157.6+020343	150.49001	2.06934	0.4385	0.4409	18.93	7.60	14	12.29	44.30	3,6
SWIRE J003847.1–433227	9.67174	−43.54514	0.3609	−1.0000	18.88	4.46	14	8.00	28.39	
SWIRE J003847.2–434822	9.68008	−43.79479	0.4804	−1.0000	19.17	7.57	26	17.11	142.17	
SWIRE J003442.1–430746	8.67131	−43.14276	0.8072	−1.0000	21.87	8.44	22	16.00	102.18	
SWIRE J022717.1–044557	36.81958	−4.74909	1.3001	−1.0000	24.04	4.43	16	11.60	69.21	7

NOTE. — Same clusters found in different fields are repeatedly listed here for completeness with the same BCG coordinates. Column (1): Cluster name given by field name and J2000 coordinates of cluster center; Column (2): R.A. (J2000) of BCG; Column (3): Decl. (J2000) of BCG; Column (4): cluster redshift estimated from the median photo- z of member galaxies; Column (5): spectroscopic redshift of the BCG if available. ‘−1.0000’ stands for not available; Column (6): BCG magnitude at i' -band (7629 Å) for the CFHT-W and CFHT-D fields, i^+ -band (7629 Å) for the COSMOS field, and r -band (6230 Å) for the SWIRE field; Column (7): overdensity level; Column (8): number of member galaxy candidates within a radius of 1 Mpc and the redshift gap of $z \pm 1.44 \sigma_{\Delta z}$. See $\sigma_{\Delta z}$ in Table 1; Column (9): cluster richness; Column (10): total luminosity of cluster member galaxies, after the local background is subtracted. It is in the i' -band for the CFHT-W and CFHT-D fields, V -band for the COSMOS field, B -band for the SWIRE field; Column (11): previous catalog containing the cluster: (1). Thanjavur et al. (2009); (2). Adami et al. (2010); (3). Olsen et al. (2007); (4). Grove et al. (2009); (5). Milkeraitis et al. (2010); (6). Finoguenov et al. (2007) for X-ray; (7). Pierre et al. (2007) for X-ray.

This table is available in its entirety in a machine-readable form in the online journal. A portion is shown here for guidance regarding the form and content.

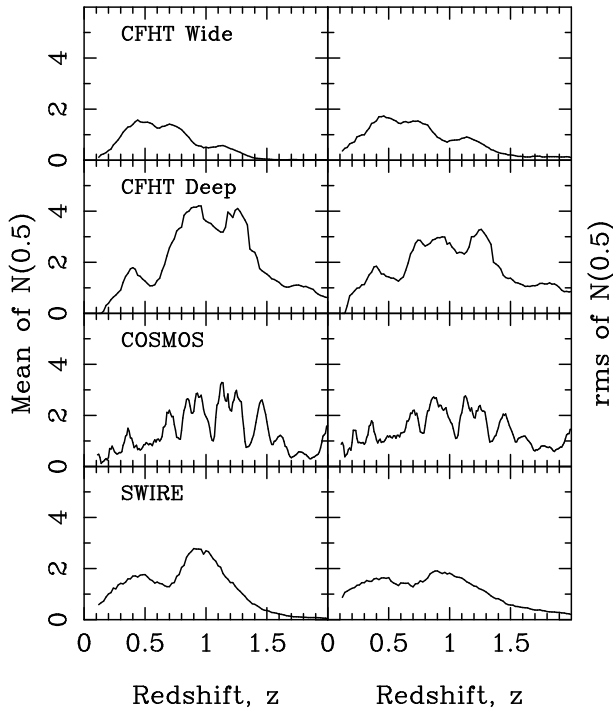


FIG. 1.— Mean and rms of background galaxies of $M_r \leq M_{lim}$ within a radius of 0.5 Mpc and a redshift gap between $z \pm 1.44 \sigma_{\Delta z}$.

limit. Here, $\langle N(0.5) \rangle$ is the mean galaxy count of the same magnitude limit within 0.5 Mpc for each field for the given redshift gap, $\sigma_{N(0.5)}$ is the root mean square (rms) of the number count (see Figure 1). In practices, 300 random positions (R.A., Decl.) are selected in the real data, and the number of luminous galaxies of $M \leq M_{lim}$ is counted within a radius of 0.5 Mpc and a redshift gap between $z \pm 1.44 \sigma_{\Delta z}$. The mean and the rms are statistically obtained from these 300 values. A larger value of D means a higher likelihood of a true cluster (see Table 2). We set the threshold, $D \geq 4$, for cluster identification. Meanwhile, we also require $N(0.5) \geq 8$ to avoid the detection of poor clusters or false detection in case that the mean number and rms of background are very small. Now, if all conditions are satisfied, a cluster is identified.

5. The real center of a detected cluster is then defined as the average position of luminous member galaxy candidates of $M \leq M_{lim}$ within radius of 1 Mpc (not 0.5 Mpc) from the temporary center and the redshift gap of $z \pm 1.44 \sigma_{\Delta z}$. This position is given in the cluster name. The cluster richness, R , is defined as the *real* number of cluster galaxies, which is obtained from the number of member galaxy candidates, N_{gal} , within a radius of 1 Mpc from the real center of a cluster and the redshift gap subtracted by the local contaminations $\langle N_{cb} \rangle$ of foreground and background galaxies, so that $R = N_{gal} - \langle N_{cb} \rangle$. The contamination, $\langle N_{cb} \rangle$, is estimated from the local distribution of the galaxies in this redshift gap (see details in Wen et al. 2009).

6. The total luminosity of each cluster, L_{tot} , is calculated as the total luminosity of member galaxies within the region after the similar subtraction of the average background contribution.

$\langle N(0.5) \rangle / \sigma_{N(0.5)}$, is estimated from the member number and the background galaxy density of the same magnitude

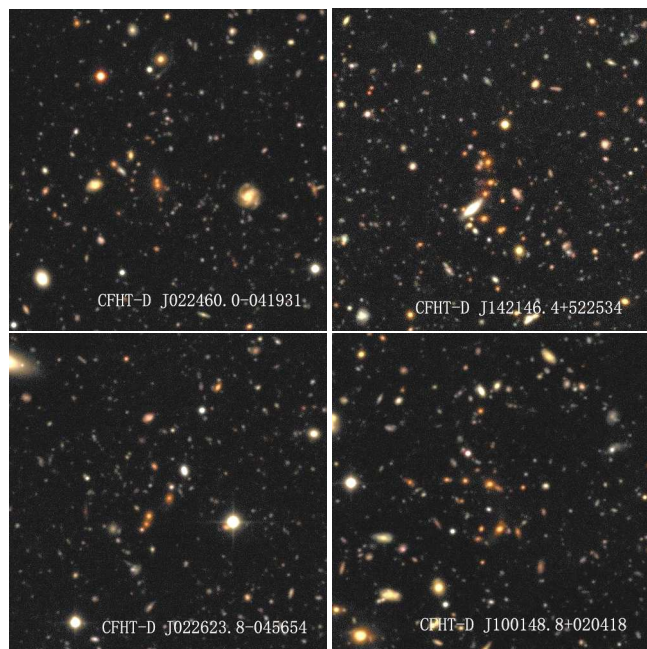


FIG. 2.— Examples for clusters in the CFHT Deep field identified only from data of Ilbert et al. (2006) (*upper*) and only from data of Coupon et al. (2009) (*bottom*). The images have a field of view of $1.5' \times 1.5'$. The most of bright red galaxies in the images are member galaxies. A color version of this figure is available in the online journal.

As listed in Table 2, we get 631 clusters from the CFHT Wide field, 187 clusters from the COSMOS field and 737 clusters from the SWIRE field. In the CFHT Deep field, two sets of photometric redshifts by Coupon et al. (2009) and Ilbert et al. (2006) are available for galaxies with similar uncertainties. Both are used for our cluster detection independently. We get 163 clusters using the photo- z data of Coupon et al. (2009) and 105 clusters using the photo- z data of Ilbert et al. (2006). Among them, 66 clusters are detected from both, 97 clusters only from Coupon et al. (2009) and 39 only from Ilbert et al. (2006). Figure 2 shows two example clusters identified only from the data of Ilbert et al. (2006) and two examples only from the data of Coupon et al. (2009). All clusters have an overdensity $D \geq 4$ in one dataset but less than 4 in the other. Merging two samples gives 202 unique clusters from the CFHT Deep field.

We notice that there are the overlapped regions between the four fields: the COSMOS field is overlapped with a part (D2) of the CFHT Deep field; a part (W1) of the CFHT Wide field is overlapped with the D1 region of the CFHT Deep field and the XMM region of the SWIRE field. Therefore, some clusters are repeatedly detected from the photometric redshift data of different fields. Merging 1757 entries of clusters in Table 2 from the four fields gives 1644 clusters in total. Among them, 1088 clusters are newly identified, and more than half of them are identified from the large SWIRE field *which has not been searched for clusters previously*. Among 228 clusters of $z \geq 1$, 191 are newly identified, and again, more than half of them are identified from the SWIRE field. See Table 1 for the numbers of clusters identified from each field.

Figure 3 shows the redshift distribution of detected clusters in each field in the range of $0.1 \lesssim z \lesssim 1.6$. The median redshifts of the clusters from the CFHT Wide, the CFHT Deep, the COSMOS and the SWIRE are 0.63, 0.86, 0.85,

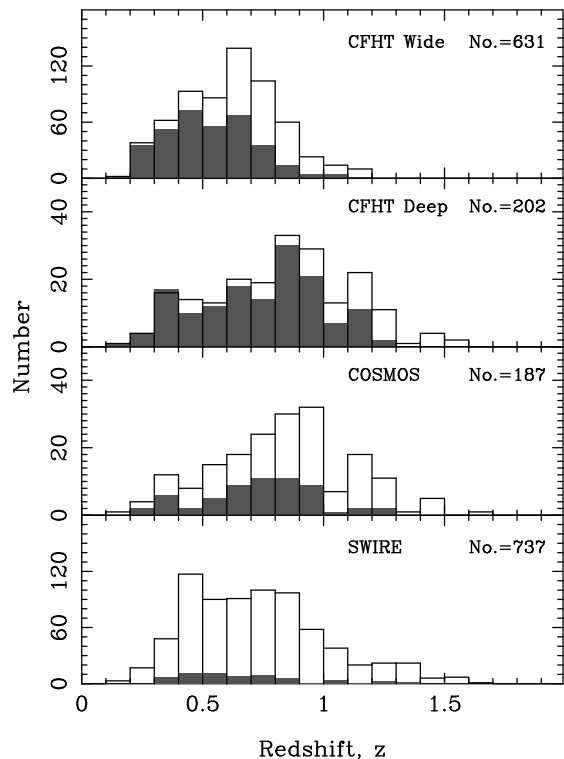


FIG. 3.— Redshift distribution of detected clusters from the four deep fields. The grey area indicates the previous known clusters in our sample.

0.70, respectively. According to the redshift distribution of clusters, clusters of $z \leq 0.7$ (i.e. less than the peak redshift) in the CFHT Wide field probably have their luminous member galaxies selected with a similar completeness. At higher redshifts, the richness is biased to a smaller value, since only the brighter galaxies can be detected because of the observational magnitude limit. Similarly, the redshift is $z \leq 0.9$ for clusters in the CFHT Deep field, $z \leq 1$ for the COSMOS field, $z \leq 0.8$ for the SWIRE field.

We check the companions within a radius of 2 Mpc and $z \pm 3 \sigma_{\Delta z}$ of the detected clusters, and find that 76% of clusters have no companion, 20% of clusters have one companion, and 4% of clusters have two companions. Companions for a small number of clusters probably indicate superclusters or the cluster mergers.

2.3. False detection rate

Because of the projection effect and the uncertainty of photo- z , it is possible that a false cluster is detected by chance in the photo- z data of galaxies by the procedures above. We have to estimate the false detection rate of our cluster detection algorithm.

Following the method of Wen et al. (2009), we perform Monte Carlo simulations based on the real data for the purpose. First, each galaxy in the real dataset is forced to have a random walk in the sky plane towards a random direction with a step length of a random value larger than 1.0 Mpc but less than 2.5 Mpc. Second, we shuffle the photo- z and absolute magnitude of all galaxies in each field. These procedures should eliminate real clusters but reserve the statistical properties of original dataset. We apply the cluster detection algorithm to such a 3-D shuffled data, to see how many “false clusters” can be detected with the criteria of $D \geq 4$

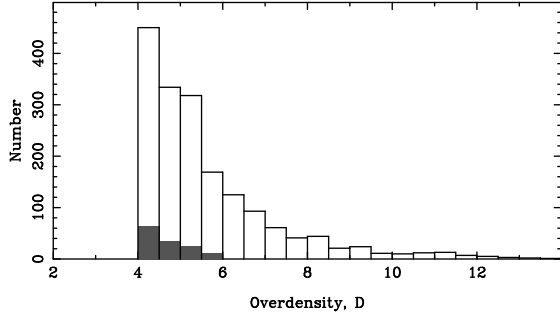


FIG. 4.— Distribution of the overdensity of detected clusters from real data and the “false” clusters from the 3-D shuffled data (grep area).

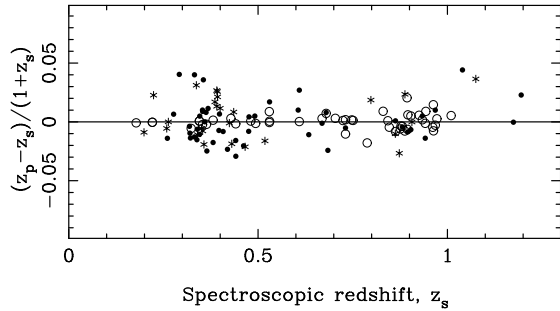


FIG. 5.— Comparison between the cluster redshift z_p (the median of photo- z of member galaxies) and the spectroscopic redshift of BCG, z_s : dots for 48 CFHT clusters with a standard deviation, $\sigma_{(z_p - z_s)/(1 + z_s)}$, of 0.017, open circles for 48 COSMOS clusters with a standard deviation of 0.006, and stars for 26 SWIRE clusters with a standard deviation of 0.018.

and $N(0.5) \geq 8$. We repeat such tests 100 times, and get the false detection rate of 9.9%, 2.9%, 3.2% and 7.9%, respectively, for the CFHT Wide data, the CFHT Deep data, the COSMOS data and the SWIRE data. Figure 4 shows the average overdensity distribution of the detected clusters from the four fields, together with that of “false clusters” from the 3-D shuffled data. The “false” clusters preferably have a low overdensity.

2.4. The brightest cluster galaxies

We recognize the BCG of a cluster as the brightest galaxy within a radius of 0.5 Mpc from the cluster center and a photo- z gap of $z \pm 1.44 \sigma_{\Delta z}$. Furthermore, we check the images of all clusters and BCGs to clean out any possible contamination, e.g., blue spiral galaxies mis-identified as BCGs and bad photometries. For the CFHT Wide and Deep clusters, we inspect the color composite CFHT images at the website¹. For the COSMOS and SWIRE clusters overlapped in the CFHT field, we view the CFHT images, otherwise the COSMOS images² or the SWIRE images³. We also inspect the SDSS color composite images⁴ for clusters of $z < 0.6$ located at the SDSS field. The coordinates and the AB magnitudes of the BCGs are given in Table 2. The AB magnitudes are taken from the data for the CFHT, the COSMOS and the XMM region of the SWIRE field. The Vega magnitudes are taken from that for the SWIRE field (except the XMM region) and are transfer to AB

¹ <http://www1.cadc-ccda.hia-ihp.nrc-cnrc.gc.ca/community/CFHTLS-SG/docs/csky.html>

² <http://irsa.ipac.caltech.edu/data/COSMOS>

³ <http://irsa.ipac.caltech.edu/data/SPITZER/SWIRE>

⁴ <http://cas.sdss.org/astrodr7/en>

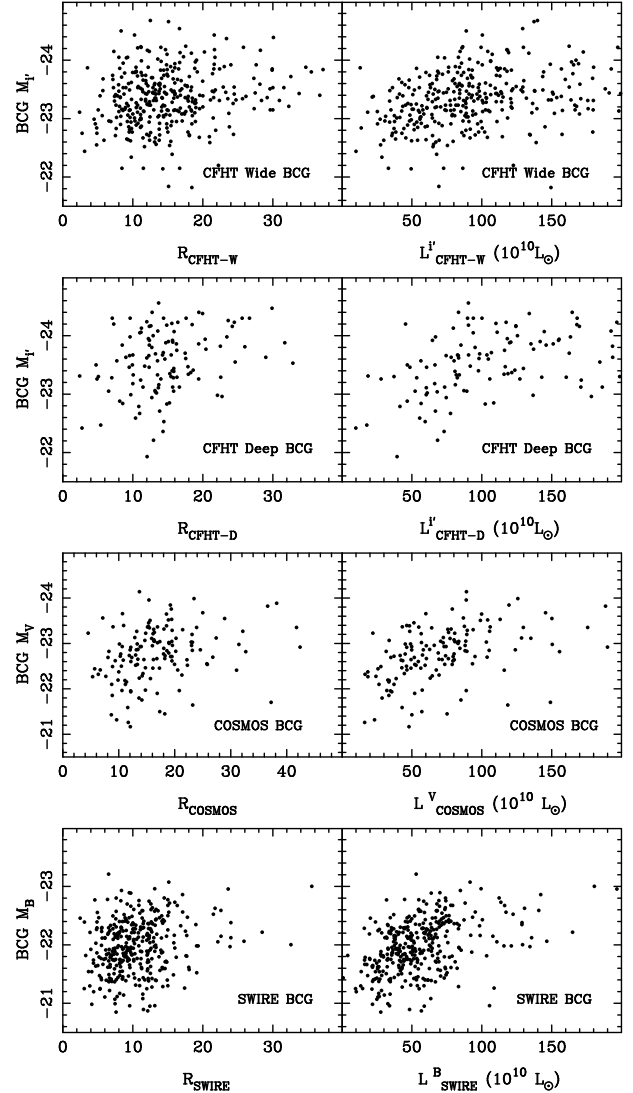


FIG. 6.— Correlations between the absolute magnitudes (i.e. the luminosities) of BCGs with the cluster richnesses and the total luminosities.

magnitude⁵ for the rest SWIRE field via $r_{AB} = r_{Vega} + 0.17$.

Because BCGs are brighter than other member galaxies, some of them have the spectroscopic redshifts obtained already, e.g. Le Fèvre et al. (2005) for the CFHT field, Lilly et al. (2007) for the COSMOS field, Rowan-Robinson et al. (2008) for the SWIRE field. We also check the spectroscopic redshifts of BCGs from the SDSS DR7 database (Abazajian et al. 2009). Figure 5 shows the difference between the median photometric redshift of cluster members and the spectroscopic redshift of BCGs, $(z_p - z_s)/(1 + z_s)$. The standard deviations roughly indicate the accuracy of redshift estimate for clusters.

The luminosities of BCGs are more or less correlated to the cluster richness and the cluster total luminosities (see Fig. 6). Richer clusters tend to have more luminous BCGs. The strongest correlation appears between absolute magnitude of the COSMOS BCG and total luminosity.

2.5. Matching for different detections

⁵ <http://www.sdss.org/dr7/algorithms/sdssUBVRITransform.html>

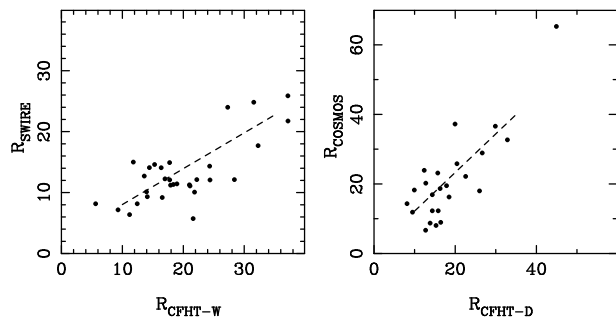


FIG. 7.— Comparison between the richnesses of matched clusters in the overlapped regions between the CFHT Wide and the SWIRE fields and between the CFHT Deep and the COSMOS with different absolute magnitude limits.

Note that the absolute magnitude limits of the member galaxy selection are different for the four deep fields (see Table 1). That is $M_{i'} = -21.5$ for the CFHT field, $M_V = -20.5$ of an aperture of $3''$ for the COSMOS field, and $M_B = -20.5$ for the SWIRE field. Different limits allow the member galaxies of different luminosities to be selected in the cluster detection algorithm. The richness of a cluster therefore depends on the absolute magnitude limits.

Clusters in some overlap regions have been detected from the dataset of two deep fields via the cluster detection algorithm, matched within a separation of 1 Mpc and a redshift difference of $\Delta z \leq 0.04(1+z)$. We compare their richnesses obtained from the two field datasets with different absolute magnitude limits at different bands, if luminous member galaxies are almost completely selected. We get 650 matched clusters in the overlapped region of the CFHT Wide field and the CFHT Deep field, 24 matched clusters in the COSMOS and CFHT Deep fields, 31 matched clusters in the SWIRE and CFHT Wide fields. Figure 7 compares the richnesses of the matched clusters obtained from the overlapped regions between the CFHT Wide and the SWIRE fields and between the CFHT Deep and the COSMOS fields. As expected, these richnesses are correlated.

As shown in the Figure 3 and mentioned in Sect. 1.1, a large amount of clusters have previously been detected in the CFHT Wide and Deep fields. For example, Olsen et al. (2007) applied a matched-filter algorithm to the i' -band four CFHT Deep fields, and identified 162 cluster candidates with an estimated redshift uncertainty of $\sigma_{\Delta z} = 0.1$. Grove et al. (2009) applied the method to the r' and z' bands the four CFHT Deep fields, and found 114 and 247 cluster candidates from the two bands, respectively. Thanjavur et al. (2009, and private communication) used a red sequence method to the CFHT Wide field of the 161 deg^2 data and found 5804 cluster candidates. Adami et al. (2010) used a 3-D method and identified 1029 clusters from the 28 deg^2 CFHT Wide field and 171 clusters from the 2.5 deg^2 CFHT Deep field with a mass greater than $1.0 \times 10^{13} M_\odot$. Milkeraitis et al. (2010) used 3D-Matched-Filter to identify clusters from the CFHT Deep fields, and found 673 clusters in the redshift range of $0.2 \leq z \leq 1.0$. We merge these previous cluster samples, and get 760 unique clusters in the CFHT Deep field, and 5848 unique clusters from the CFHT Wide field. We match those with our sample by a separation of 1 Mpc and a redshift difference of $\Delta z \leq 0.2$, and get 346 matched clusters in the CFHT Wide field, and 144 matched clusters in the CFHT Deep field. In Figure 8, we compare the distribution of known clusters and

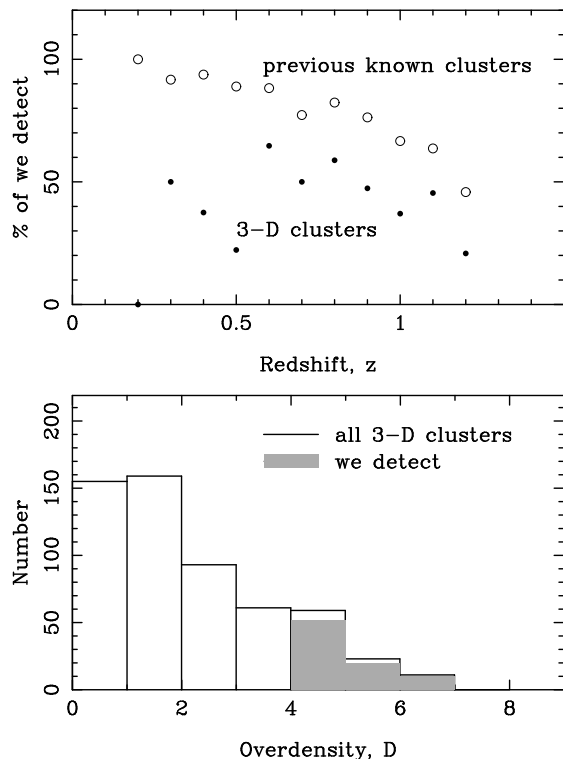


FIG. 8.— Known clusters and our detections. *Upper panel*: the percentage of our detected clusters are previously known in the CFHT Deep field (open circle), especially by 3-D methods (black dots) in Adami et al. (2010) and Milkeraitis et al. (2010). *Lower panel*: the number of the 3-D clusters we detect. Apparently we detect the 3-D clusters of only a high overdensity.

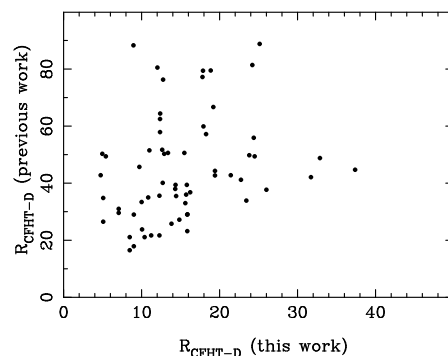


FIG. 9.— Comparison of the richnesses of matched clusters we define by the number of luminous galaxies with those given in Olsen et al. (2007) and Grove et al. (2009) defined as the average number of L^* galaxies based on a single band photometric data. Here L^* is the characteristic luminosity in the Schechter luminosity function.

our detections. At low redshifts, almost all clusters we detect are known previously. However, we detect some new clusters at high redshifts which are not previously known. Among the clusters detected by the 3-D method (Adami et al. 2010; Milkeraitis et al. 2010), we detect only those rich ones in general which have a high overdensity of $D \geq 4$.

In Figure 9, we compare our richnesses of matched clusters of $z \leq 0.9$ in the CFHT Deep field with the richness given by Olsen et al. (2007) and Grove et al. (2009) as the equivalent number of L^* galaxies, based on photometric data of a single band, here L^* is the characteristic luminosity in the Schechter luminosity function. Though with a large scatter, richer clusters found by previous authors show a larger richness by our

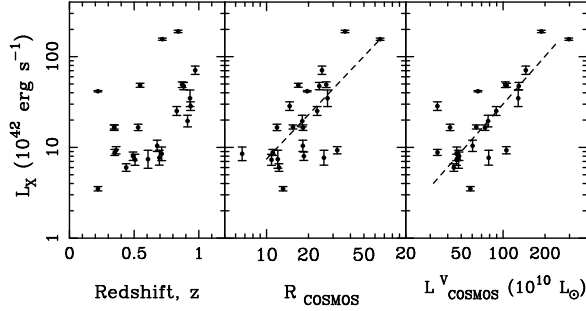


FIG. 10.— Correlations of the X-ray luminosity with the cluster richness, R_{COSMOS} , (the middle panel) and the total V -band luminosity, L_{COSMOS}^V , (the right panel) with for 24 COSMOS clusters in the redshift range of $0.2 < z < 1.0$ (see the left panel).

definition.

2.6. X-ray emission of clusters

Some clusters in the COSMOS field have X-ray emission detected. Using the XMM-Newton data, Finoguenov et al. (2007) identified 72 X-ray clusters in the 1.7 deg^2 of the COSMOS field, 24 of which are matched with our sample within a projected separation of $r_p < 1 \text{ Mpc}$ and a redshift difference of $\Delta z \leq 0.05$ ($\sim 2\sigma$ of the cluster redshift uncertainty in Finoguenov et al. 2007). These X-ray clusters have a redshift in the range of $0.2 < z < 1$ (see Figure 10).

Similar to low-redshift galaxy clusters (Wen et al. 2009), significant correlations are found between the X-ray luminosity of clusters and the cluster richness (R , the middle panel of Figure 10) or the total V -band luminosity (L_V , the right panel of Figure 10). The best fittings to the data give

$$\log L^{X,42} = (-0.75 \pm 0.43) + (1.62 \pm 0.34) \log R_{\text{COSMOS}}, \quad (1)$$

and

$$\log L^{X,42} = (-2.02 \pm 0.48) + (1.75 \pm 0.26) \log L_{\text{COSMOS}}^{V,10}, \quad (2)$$

where $L^{X,42}$ refers to X-ray luminosity in the 0.1–2.4 keV band in unit of $10^{42} \text{ erg s}^{-1}$, $L_{\text{COSMOS}}^{V,10}$ refers to the total V -band luminosity in unit of $10^{10} L_{\odot}$ from the COSMOS measurements. The correlations suggest that the richness we define closely relates to the properties of clusters.

3. STELLAR POPULATION AND COLOR EVOLUTION OF BCGs

The colors of BCGs provide important information on their stellar population. Since the clusters in our sample have large redshifts, one can easily study the stellar population and color evolution of these BCGs. Here, we work on color evolution as a function of redshift, in the light of a stellar population synthesis model.

For the CFHT data, the BCG magnitudes at $u'g'r'i'z'$ bands are available from Coupon et al. (2009). The r' (7480 Å) and z' (8930 Å) bands correspond to the rest-frame optical wavelength for observed BCGs up to redshift $z \sim 1$, and the g' band (4860 Å) corresponds to the rest-frame optical wavelength at low redshifts and the UV wavelength at high redshifts. The BCG magnitudes at the r' , z' and g' bands are used to define the BCG colors for the clusters in the CFHT Wide and Deep fields, as shown in Figure 11 and Figure 12.

To explain the color changes, we show the evolution lines calculated by using the stellar population synthesis models

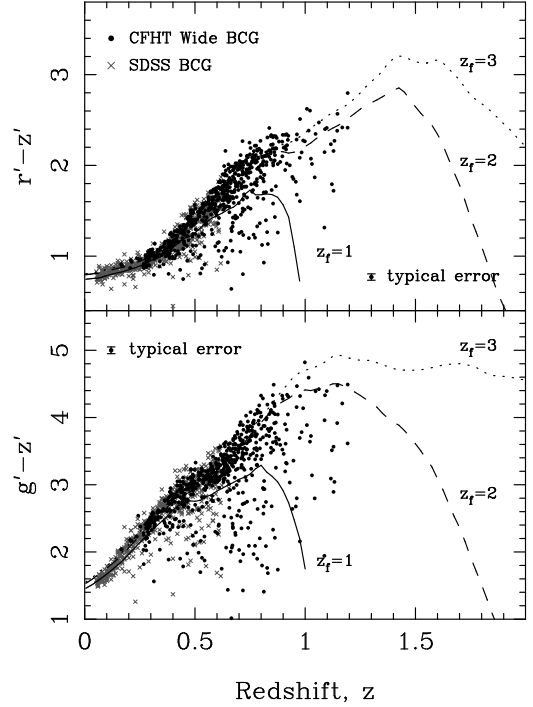


FIG. 11.— The colors, $g' - z'$, $r' - z'$ as a function of redshift for BCGs in the CFHT Wide field. Three lines represent the color evolution with redshift from a model of passively evolved galaxies formed at redshift $z_f = 1$ (solid line), $z_f = 2$ (dashed line) and $z_f = 3$ (dotted line), respectively. To outline the evolution at lower redshifts ($z < 0.6$), the same-color data of 500 BCGs from the SDSS clusters in Wen et al. (2009) are included in the plots.

(Bruzual & Charlot 2003, BC03, hereafter). We adopt the stellar evolution tracks of Padova 1994 (Girardi et al. 1996), the Basel3.1 stellar spectral library (Westera et al. 2002), and the initial mass function of Chabrier (2003) and the Solar metallicity. The solid line in Figure 11 stands for the color evolution for a galaxy formed at redshift $z_f = 1$ and evolved passively with cosmic time, and the dashed and dotted lines for galaxies formed at redshift $z_f = 2$ and 3, respectively. We find that the BCG color⁶, $r' - z'$, is consistent with the BC03 model of $z_f = 2$ and 3, but significant redder than that of $z_f = 1$. The BCG color, $g' - z'$, of $z \lesssim 0.8$ is consistent with models of $z_f = 2$ and 3, but significant bluer than the models at higher redshift.

For the COSMOS data, the B (4440 Å), r^+ (6232 Å) and $m_{3.6\mu\text{m}}$ bands are used to define the BCG colors. The B and r^+ band data are available from Ilbert et al. (2009). The B band corresponds to the rest-frame optical wavelength at low redshifts, but the rest-frame UV wavelength at high redshifts. We obtain the $3.6\mu\text{m}$ flux within an aperture of $1.9''$ diameter from the Spitzer S-COSMOS survey (Sanders et al. 2007). Since the optical fluxes are measured over an aperture of $3''$ in diameter which encloses 75% of the flux for a point-like source, we therefore convert the $3.6\mu\text{m}$ flux following Ilbert et al. (2009) to match the aperture of optical data. The AB magnitude at $3.6\mu\text{m}$ is then calculated via equation,

⁶ When comparing the color data with model, we have to systematically add 0.1 to $r' - z'$ and 0.2 to $g' - z'$ of BCGs in the CFHT Wide field (see Figure 11) to get consistence at low redshift ($z \lesssim 0.3$). For the BCGs from the CFHT Deep field in Figure 12, we have to systematically add 0.2 to $r' - z'$ and 0.3 to $g' - z'$. These calibrations are necessary to compensate the possible systematical bias in photometric data of different bands.

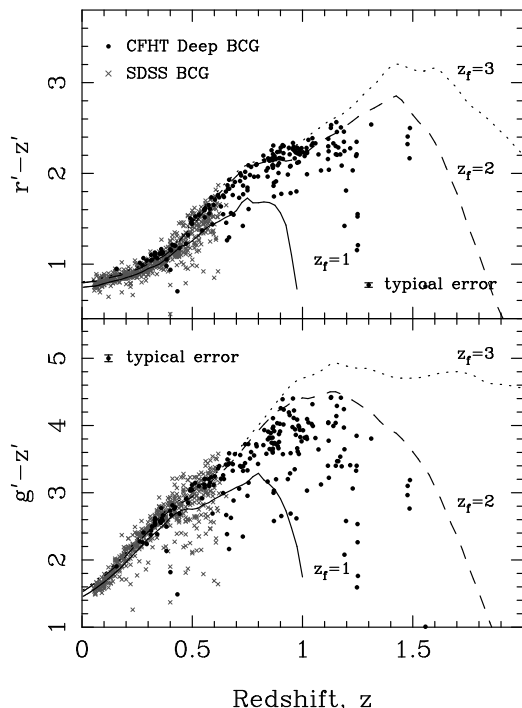


FIG. 12.— The same as Figure 11 but for BCGs of clusters found in the CFHT Deep field.

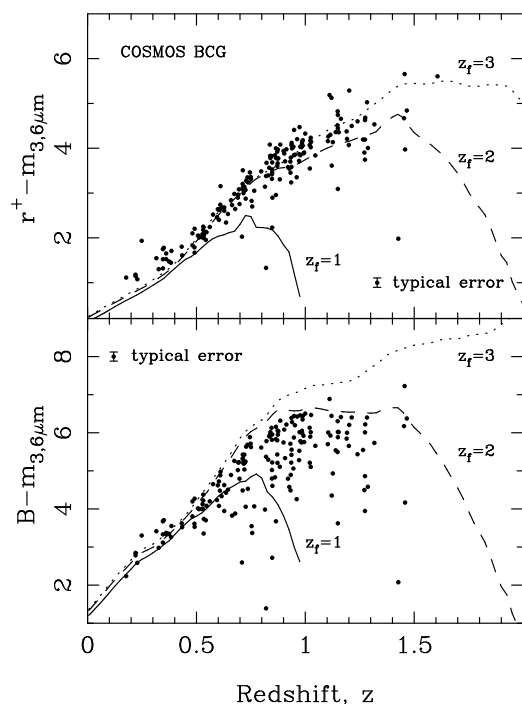


FIG. 13.— The color evolution of BCGs in the COSMOS field. The lines are calculated from the BC03 model as the same as Figure 11 but for the colors, $r^+ - m_{3.6\mu m}$ and $B - m_{3.6\mu m}$.

$m_{3.6\mu m} = 23.9 - 2.5 \log(f_{3.6\mu m})$, where $f_{3.6\mu m}$ is in unit of μJy .

Figure 13 shows the color evolution of BCGs in the COSMOS field. We find that the color, $r^+ - 3.6\mu m$, is consistent with the BC03 model for $z_f = 2$ and 3. The color data of $B - m_{3.6\mu m}$ at $z < 0.5$ is consistent with that of models of

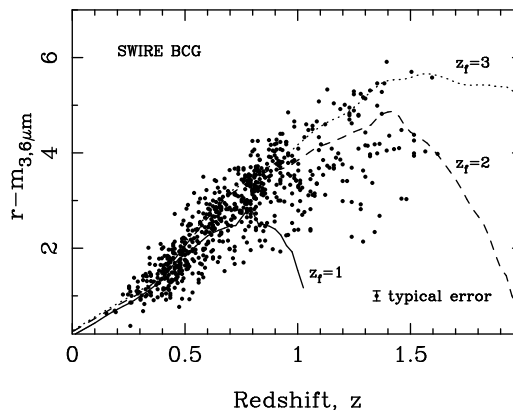


FIG. 14.— The color evolution of BCGs in the Spitzer SWIRE field. The lines are calculated from the BC03 model as Figure 11 but for the color of $r - m_{3.6\mu m}$.

$z_f = 2$ and 3, but significant bluer than the models at higher redshift.

For the SWIRE data, the magnitudes of r and $3.6\mu m$ bands are available from Rowan-Robinson et al. (2008) and are used for color evolution study (see Figure 14). The result is consistent with that from the COSMOS clusters.

The wavelengths of r' , z' , r^+ and $m_{3.6\mu m}$ bands correspond the optical or infrared band in the rest-frame, and the observed emission of galaxies in these bands is dominated by old stellar populations. The color evolution shown by these high redshift data shows that the stellar population in most BCGs have been formed at $z \geq 2$, in agreement with Stott et al. (e.g., 2008) and Whiley et al. (2008). The data of colors $g' - z'$ and $B - m_{3.6\mu m}$ at high redshifts in Figure 11–13 are related to the enhancement rest-frame UV color which indicates star formation in the high redshift BCGs (Donahue et al. 2010; Hicks et al. 2010).

4. CONCLUSIONS

Using the photo- z data of the four deep fields, we identified 631 clusters, 202 clusters, 187 clusters and 737 clusters, respectively, from the CFHT Wide field, the CFHT Deep field, the COSMOS field and the SWIRE fields. Clusters are recognized when an overdensity is $D \geq 4$ and more than eight luminous galaxies are found within a radius of 0.5 Mpc and a photo- z gap. These clusters have redshifts in the range of $0.1 \lesssim z \lesssim 1.6$. Because of overlapping areas among the four fields, merging these cluster samples gives 1644 clusters, of which 1088 clusters are newly identified and 228 clusters have a redshift $z \geq 1.0$. The false detection rate is estimated to be less than 10%. The cluster redshift is estimated as the median photo- z of member galaxies. Richer clusters tend to have more luminous BCGs. The cluster richness and total luminosity are tightly related to the X-ray luminosity.

The BCG colors and their evolution are studied for the large sample clusters in the four fields. We compared them with a passive galaxy evolution model using the stellar population synthesis. The color evolution is consistent with the BC03 model in which the stars in BCGs are formed at $z_f \geq 2$ and evolved passively. The systematical enhancement rest-frame UV color indicates star formation in these BCGs.

We thank the referee for helpful comments, especially the 100 3-D shuffled samples for checking the false detection

rate. We are grateful to Dr. Yanbin Yang for help of understanding BC03 model and valuable discussions. We also thank K. Thanjavur and M. Milkeraitis for providing their CFHT cluster samples. The authors are supported by the Na-

tional Natural Science foundation of China (10821061 and 10833003), the National Key Basic Research Science Foundation of China (2007CB815403).

REFERENCES

- Abazajian, K. N., et al. 2009, *ApJS*, 182, 543
 Abell, G. O., Corwin, Jr., H. G., & Olowin, R. P. 1989, *ApJS*, 70, 1
 Adami, C., et al. 2010, *A&A*, 509, A81
 Andreon, S., de Propris, R., Puddu, E., Giordano, L., & Quintana, H. 2008, *MNRAS*, 383, 102
 Aragon-Salamanca, A., Baugh, C. M., & Kauffmann, G. 1998, *MNRAS*, 297, 427
 Ascaso, B., et al. 2011, *ApJ*, 726, 69
 Bahcall, N. A. 1988, *ARA&A*, 26, 631
 Bahcall, N. A., Fan, X., & Cen, R. 1997, *ApJ*, 485, L53
 Bernardi, M. 2009, *MNRAS*, 395, 1491
 Bildfell, C., Hoekstra, H., Babul, A., & Mahdavi, A. 2008, *MNRAS*, 389, 1637
 Bremer, M. N., et al. 2006, *MNRAS*, 371, 1427
 Brodwin, M., et al. 2006, *ApJ*, 651, 791
 Brodwin, M., et al. 2010, *ApJ*, 721, 90
 Bruzual, G. & Charlot, S. 2003, *MNRAS*, 344, 1000
 Butcher, H. & Oemler, Jr., A. 1978, *ApJ*, 219, 18
 —. 1984, *ApJ*, 285, 426
 Cardamone, C. N., et al. 2010, *ApJS*, 189, 270
 Castellano, M., et al. 2007, *ApJ*, 671, 1497
 Castillo-Morales, A. & Schindler, S. 2003, *A&A*, 403, 433
 Chabrier, G. 2003, *PASP*, 115, 763
 Chiaberge, M., et al. 2010, *ApJ*, 710, L107
 Coe, D., Benítez, N., Sánchez, S. F., Jee, M., Bouwens, R., & Ford, H. 2006, *AJ*, 132, 926
 Collins, C. A. & Mann, R. G. 1998, *MNRAS*, 297, 128
 Coupon, J., et al. 2009, *A&A*, 500, 981
 Croft, S., de Vries, W., & Becker, R. H. 2007, *ApJ*, 667, L13
 Csabai, I., et al. 2003, *AJ*, 125, 580
 De Lucia, G. & Blaizot, J. 2007, *MNRAS*, 375, 2
 Demarco, R., et al. 2010, *ApJ*, 711, 1185
 Donahue, M., et al. 2010, *ApJ*, 715, 881
 Dressler, A. 1980, *ApJ*, 236, 351
 Egami, E., Rieke, G. H., Fadda, D., & Hines, D. C. 2006, *ApJ*, 652, L21
 Eisenhardt, et al. 2008, *ApJ*, 684, 905
 Fassbender, R., et al. 2008, *A&A*, 481, L73
 Finoguenov, A., et al. 2007, *ApJS*, 172, 182
 Finoguenov, A., et al. 2010, *MNRAS*, 403, 2063
 Fukugita, M., Shimasaku, K., & Ichikawa, T. 1995, *PASP*, 107, 945
 Gilbank, D. G., et al. 2008, *ApJ*, 677, L89
 Gillis, B. R. & Hudson, M. J. 2011, *MNRAS*, 410, 13
 Girardi, L., Bressan, A., Chiosi, C., Bertelli, G., & Nasi, E. 1996, *A&AS*, 117, 113
 Gladders, M. D. & Yee, H. K. C. 2005, *ApJS*, 157, 1
 Goto, T., et al. 2008, *PASJ*, 60, 531
 Grove, L. F., Benoist, C., & Martel, F. 2009, *A&A*, 494, 845
 Hao, J., et al. 2010, *ApJS*, 191, 254
 Hicks, A. K., Mushotzky, R., & Donahue, M. 2010, *ApJ*, 719, 1844
 Hoyle, B., Jimenez, R., & Verde, L. 2010, *arXiv:1009.3884*
 Hsieh, B. C., Yee, H. K. C., Lin, H., & Gladders, M. D. 2005, *ApJS*, 158, 161
 Ilbert, O., et al. 2006, *A&A*, 457, 841
 Ilbert, O., et al. 2009, *ApJ*, 690, 1236
 Knobel, C., et al. 2009, *ApJ*, 697, 1842
 Kurk, J., et al. 2009, *A&A*, 504, 331
 Lauer, T. R., et al. 2007, *ApJ*, 662, 808
 Le Fèvre, O., et al. 2005, *A&A*, 439, 845
 Lilly, S. J., et al. 2007, *ApJS*, 172, 70
 Liu, F. S., Mao, S., Deng, Z. G., Xia, X. Y., & Wen, Z. L. 2009, *MNRAS*, 396, 2003
 Liu, F. S., Wen, Z. L., Han, J. L., & Meng, X. M. 2011, *SCIENCE CHINA*, in press (*arXiv:1012.5959*)
 Liu, F. S., Xia, X. Y., Mao, S., Wu, H., & Deng, Z. G. 2008, *MNRAS*, 385, 23
 Lonsdale, C. J., et al. 2003, *PASP*, 115, 897
 Matarrese, S., Verde, L., & Jimenez, R. 2000, *ApJ*, 541, 10
 McMahon, R. G., et al. 2001, *New Astronomy Review*, 45, 97
 McNamara, et al. 2006, *ApJ*, 648, 164
 Miley, G. K., et al. 2006, *ApJ*, 650, L29
 Milkeraitis, M., et al. 2010, *MNRAS*, 406, 673
 Mobasher, B., et al. 2004, *ApJ*, 600, L167
 Mullis, C. R., et al. 2005, *ApJ*, 623, L85
 Muzzin, A., et al. 2009, *ApJ*, 698, 1934
 Negrello, M., et al. 2009, *MNRAS*, 394, 375
 O’Dea, C. P., et al. 2008, *ApJ*, 681, 1035
 Olsen, L. F., et al. 2007, *A&A*, 461, 81
 Papovich, C., et al. 2010, *ApJ*, 716, 1503
 Pelló, et al. 2009, *A&A*, 508, 1173
 Pierre, M., et al. 2007, *MNRAS*, 382, 279
 Postman, M., Huchra, J. P., & Geller, M. J. 1992, *ApJ*, 384, 404
 Reiprich, T. H. & Böhringer, H. 2002, *ApJ*, 567, 716
 Rines, K., Finn, R., & Vikhlinin, A. 2007, *ApJ*, 665, L9
 Rowan-Robinson, M., et al. 2008, *MNRAS*, 386, 697
 Sanders, D. B., et al. 2007, *ApJS*, 172, 86
 Stanford, S. A., et al. 2005, *ApJ*, 634, L129
 Stanford, S. A., et al. 2006, *ApJ*, 646, L13
 Stott, J. P., et al. 2010, *ApJ*, 718, 23
 Stott, J. P., Edge, A. C., Smith, G. P., Swinbank, A. M., & Ebeling, H. 2008, *MNRAS*, 384, 1502
 Thanjavur, K., Willis, J., & Crampton, D. 2009, *ApJ*, 706, 571
 van Breukelen, C., et al. 2006, *MNRAS*, 373, L26
 Vikhlinin, A., et al. 2009, *ApJ*, 692, 1060
 Wang, Y., Park, C., Hwang, H. S., & Chen, X. 2010, *ApJ*, 718, 762
 Wen, Z. L., Han, J. L., & Liu, F. S. 2009, *ApJS*, 183, 197
 —. 2010, *MNRAS*, 407, 533
 Westera, P., Lejeune, T., Buser, R., Cuisinier, F., & Bruzual, G. 2002, *A&A*, 381, 524
 Whiley, I. M., et al. 2008, *MNRAS*, 387, 1253
 Wilson, G., et al. 2009, *ApJ*, 698, 1943
 Zatloukal, M., Röser, H., Wolf, C., Hippelein, H., & Falter, S. 2007, *A&A*, 474, L5